Journal of Inflammation Research

Dovepress
Taylor & Francis Group

Open Access Full Text Article

ORIGINAL RESEARCH

CD8$^+$ T Cell-Derived Perforin Exacerbates Dysbiosis and Inflammatory Bowel Disease via β-Hydroxybutyrate Suppression in Mouse Colonic Epithelium

Shiyang Huang[1,2,*], Lehan Pan[3–5,*], Mingyang Li[1,2], Shu Pang[4–7], Yue Tian[8], Wen Shi[1,2], Ye Zong[4–6], Dong Zhang[8–10], Dan Tian[3–5]

[1]Immunology Research Center for Oral and Systemic Health, Beijing Clinical Research Institute, Beijing Friendship Hospital, Capital Medical University, Beijing, People's Republic of China; [2]Beijing Key Laboratory of Tolerance Induction and Organ Protection in Transplantation, Beijing Friendship Hospital, Capital Medical University, Beijing, People's Republic of China; [3]Department of General Surgery, Beijing Friendship Hospital, Capital Medical University, Beijing, People's Republic of China; [4]National Clinical Research Center for Digestive Diseases, Beijing, People's Republic of China; [5]State Key Laboratory of Digestive Health, Beijing Friendship Hospital, Capital Medical University, Beijing, People's Republic of China; [6]Department of Gastroenterology, Beijing Friendship Hospital, Capital Medical University, Beijing, People's Republic of China; [7]Department of General Practice, Beijing Friendship Hospital, Capital Medical University, Beijing, People's Republic of China; [8]Medical Research Center, Beijing Chaoyang Hospital, Capital Medical University, Beijing, People's Republic of China; [9]Beijing Institute of Brain Disorders, Capital Medical University, Beijing, People's Republic of China; [10]Beijing Laboratory of Oral Health, Capital Medical University School of Basic Medicine, Beijing, People's Republic of China

*These authors contributed equally to this work

Correspondence: Dan Tian; Dong Zhang, Email tiand@ccmu.edu.cn; zhangd@ccmu.edu.cn

Background: The etiology and pathogenesis of inflammatory bowel disease (IBD) are generally thought to be related to immune dysfunction and intestinal microbiota dysbiosis. However, the exact mechanisms remain unclear.

Methods: We applied a DSS-induced colitis model in wild-type and perforin-deficient (*Prf1*$^{-/-}$) mice. Adoptive transfer experiments and metabolic profiling were conducted, and 16S rRNA gene sequencing analyzed gut microbiota. The impact of a 3-hydroxy-3-methylglutaryl-CoA synthase 2 (HMGCS2) inhibitor on inflammation and dysbiosis was also assessed.

Results: In this study, we demonstrated that perforin production in CD8$^+$ T cells was significantly increased in both patients with IBD and mice with colitis. Moreover, compared with wild-type mice, perforin deficiency (*Prf1*$^{-/-}$) mice exhibited mitigated inflammation in a DSS-induced colitis model. The CD8$^+$ T cell adoptive transfer model indicated that perforin produced by CD8$^+$ T cells directly induced colitis. *Prf1*$^{-/-}$ mice with colitis exhibited activation of the fatty acid metabolic process, highlighted by increased expression of *Hmgcs2* and pyruvate dehydrogenase kinase isoform 4 (*Pdk4*) in the colon and accumulation of the related metabolite β-hydroxybutyrate. The absence of perforin partly reversed the imbalance in the gut microbiota composition caused by DSS, including increases in *Alloprevotella* and *Parabacteroides*. However, the HMGCS2 inhibitor exacerbated intestinal inflammation and dysbiosis in *Prf1*$^{-/-}$ mice.

Conclusion: CD8$^+$ T cell-derived perforin promoted colitis by disrupting gut microbiota composition through the suppression of β-hydroxybutyrate production. This study provides novel targets for therapeutic strategies of IBD.

Keywords: perforin, CD8$^+$ T cells, inflammatory bowel disease, microbiomes, β-hydroxybutyrate

Introduction

Inflammatory bowel disease (IBD), including ulcerative colitis (UC) and Crohn's disease (CD), is a chronic relapsing inflammatory disorder of the gastrointestinal tract that is characterized pathologically by intestinal inflammation and epithelial injury.[1,2] Recent advances have provided substantial insight into the pathogenesis of IBD, including genetic susceptibility and environmental and microbial factors.[3]

Received: 2 December 2024
Accepted: 19 April 2025
Published: 1 May 2025

Available evidence suggests that aberrant immune responses are responsible for the disease in genetically susceptible individuals.[4] Numerous pieces of evidence support the contribution of T cells in IBD, which trigger damage to intestinal cells or extracellular components through the secretion of proinflammatory cytokines.[4] Researchers have focused primarily on the association of $CD4^+$ T cells, while increasing attention is being given to the role of $CD8^+$ T cells with a deepening understanding of IBD pathogenesis. Even in colitis models where the immune system is elicited (such as ICI colitis), the most involved cell population is $CD8^+$ T cells.[5,6] The number of activated $perforin^+CD8^+$ T cells increases in the affected intestinal mucosa during the active stages of the disease course of IBD.[7] Working synergistically with granzyme molecules, perforin is a classical effector expressed by $CD8^+$ T cells, resulting in the release of cytokines and damage to target cells.[8] The activation of $CD8^+$ T cells can lead to intestinal mucosal damage and inflammation, disrupting the balance and function of gut microbiota.[9,10]

Intestinal inflammation, host metabolites and gut microbiota exhibit close and intricate interactions and mutual regulation. Patients with IBD often exhibit dysbiosis, characterized by changes in the relative abundance of certain bacterial groups, decreased microbial diversity, and alterations in metabolites.[11] Changes in metabolites can also affect the homeostasis and immune responses of intestinal mucosa. For example, the biosynthesis-related gene cluster for indoleacrylic acid is decreased in the gut metagenomes of patients with IBD, potentially contributing to barrier dysfunction.[12] Butyrate promotes mucin production by goblet cells to enhance mucosal barrier function and inhibits neutrophil-related immune responses to ameliorate mucosal inflammation in DSS-induced colitis mice.[13,14] Given the importance of gut metabolites and microbiota in the pathogenesis of IBD, further understanding the mechanisms and interactions between the microbiota and intestinal metabolism is crucial for exploring potential therapeutic approaches.

Methods

Human Tissue and Cells and Clinical Information

This study was approved by the ethics committees of Beijing Friendship Hospital, Capital Medical University (2022-P2 -428-01). Patients with IBD and healthy volunteers were recruited from Beijing Friendship Hospital between February 2023 and December 2023. The demographic and clinical characteristics of the healthy volunteers and patients with IBD were shown in Supplementary Table 1. All the subjects provided written informed consent to participate in the study. Adult outpatients and inpatients aged 18 to 70 years were potentially eligible for inclusion. Those who were diagnosed with IBD according to the "Consensus Opinions on Diagnosis and Treatment of Inflammatory Bowel Disease (2018·Beijing)" standards and who provided clinical information relevant to IBD and provided specimens were included in the study. The exclusion criteria included the following: an unclear diagnosis of IBD; the presence of abdominal organ tumors in the past three years; the use of immunosuppressive drugs within the past year; the presence of serious primary diseases of the liver, kidney, or hematopoietic system; or poor control of diabetes, AIDS, hepatitis B or rheumatic immune-related diseases. All information regarding IBD patients was categorized and presented in the Supplementary Table 2. Peripheral blood (approximately 4 mL) was collected from the participants. Peripheral blood mononuclear cells (PBMCs) were isolated by diluting the blood sample 1:1 with phosphate-buffered saline (PBS) and layering over Human Lymphocyte Separation Medium (Dakewe, 7111011).

Mice

C57BL/6J mice, B6. *Rag2/Il2rg* compound mutant ($Rag2^{-/-}\gamma c^{-/-}$) and B6. *Prf1*-knockout ($Prf1^{-/-}$) mice were purchased from The Jackson Laboratory. *Prf1/IRES-EGFP-T2A-Cre* mice were generated on the C57BL/6 background by the Shanghai Model Organisms Center as previously described.[15] In all the experiments, age- and sex-matched littermates were used. The mice were 6–8 weeks of age at the beginning of the experiments and were maintained in a specific pathogen-free, temperature-controlled environment with a 12 h light/dark cycle at Beijing Friendship Hospital. All the data derived from the animal studies were analyzed by an experimenter who was blinded to the experimental conditions. All animal experiments were approved by the Institutional Animal Care and Ethics Committee of Beijing Friendship Hospital. All the experimental procedures were performed following the Guidelines for the Care and Use of Laboratory Animals formulated by the Ministry of Science and Technology of the People's Republic of China.

DSS-Induced Colitis Model

Six to eight-week-old mice were given 2.5% dextran sulfate sodium (DSS, w/v, 36-50 kDa, MP Biomedicals) in the drinking water for 7 days. The disease activity index was calculated as previously described[16] (Supplementary Table 3). The mice in the colitis model were weighed and sacrificed at the indicated time points. Colon tissues were collected for further analyses.

$CD8^+$ T-Cell Transfer-Induced Colitis Model

Total lymphoid cells were obtained from the spleens of C57BL/6J or *Prf1*$^{-/-}$ mice and resuspended in ice-cold RPMI 1640. The suspensions were filtered through a 70 μm cell filter. Erythrocytes were eliminated with erythrocyte lysis buffer (Qiagen, 79217). The lysis process was halted by adding PBS containing 2% FBS. T lymphocytes were subsequently enriched using the Mouse $CD3^+$ T-cell Enrichment Column Kit (R&D, MTCC-25). The samples were stained with anti-PE antibody cocktail (anti-mouse TER119/CD25/CD19/CD4/CD44/NK1.1/CD11b/TCRγδ) and then incubated with anti-PE MicroBeads (Miltenyi, 130-048-801). Negative selection was performed using LS Columns (Miltenyi, 130-042-401), resulting in the isolation of naïve $CD8^+$ T cells. The purity of the naïve $CD8^+$ T cells was consistently > 90%. Eight-week-old male *Rag2*$^{-/-}$*γc*$^{-/-}$ mice were intravenously injected with 1×10^6 naïve $CD8^+$ T cells and euthanized 6 weeks after adoptive transfer.

Plasma Collection

Ten microliters of 0.5 M EDTA was added as an anticoagulant to a 1.5 mL EP tube for blood collection. The mice were anesthetized with pentobarbital sodium (50 mg/kg), and blood was promptly collected from the eyeballs. The plasma was isolated by centrifugation at 3000×g for 5 minutes.

Enzyme-Linked Immunosorbent Assay (ELISA)

ELISA was performed according to the manufacturer's instructions. A β-Hydroxybutyrate (Ketone Body) Colorimetric Assay Kit (Cayman, 700190) was used to evaluate β-hydroxybutyrate production. The plates were read with a Varioskan LUX instrument (Thermo Fisher Scientific).

Histological Analysis

The mice were anesthetized with pentobarbital sodium (50 mg/kg). Colons were removed, fixed in 4% paraformaldehyde, dehydrated in graded ethanol solutions, and embedded in paraffin. Sections were stained with hematoxylin and eosin.

Bioinformatic Analyses of RNA-Sequencing Data

Total RNA extracted from the entire colon was obtained via RNeasy Plus Micro Kit (Qiagen, Germany) and sequenced using a standard Illumina protocol (Annoroad Gene Technology, Beijing). The RNA quality was assessed utilizing a 2100 Bioanalyzer (Agilent), and the RNA concentration was quantified by an ND-2000 spectrophotometer (NanoDrop Technologies). Only RNA samples of exceptional quality, including those with an OD260/280 ratio within the range of 1.8–2.2, an OD260/230 ratio exceeding 2.0, an RNA integrity number (RIN) of 6.5 or higher, a 28S:18S ratio of at least 1.0, and a quantity exceeding 10 μg, were further processed before being used in the construction of the sequencing library. Reads were acquired on Illumina NovaSeq 6000 and mapped to the mouse genome (Mm9) by HISAT2. Gene counts were estimated by HTSeq. The R package DESeq2 was used to identify differentially expressed genes (DEGs). Genes with an adjusted P value<0.05 and a fold change>2 were defined as DEGs. The R (version 4.0.2) package clusterProfiler was used to perform gene set enrichment analysis (GSEA) of the DEGs. The sequencing data from this study can be found at the China National Center for Bioinformation (CNCB) under accession number PRJCA026385.

Reverse Transcription and Real-Time PCR

Fresh mouse tissues were submerged in RNAlater (Thermo Fisher Scientific) at 4 °C overnight. Total RNA was extracted from tissues using TRIzol Reagent (Sigma–Aldrich), after which equal amounts (1 μg) were reverse

transcribed to cDNA using the PrimeScript Reagent Kit (TaKaRa). After reverse transcription, real-time PCR amplification was performed by SYBR Green 2× PCR Mastermix (Yeason) on an Applied Biosystems 7500 Real-Time PCR System (Thermo Fisher Scientific). The PCR program consisted of 95 °C for 5 min; 40 cycles of 95 °C for 10s, 60 °C for 30s, and 72 °C for 30s; and 72 °C for 5 min. The expression levels of candidate genes were normalized to those of GAPDH. The primer sequences utilized for PCR amplification were detailed in Supplementary Table 4.

Isolation of Colonic Cells

Colons removed of fecal contents were opened longitudinally and cut into 1 cm pieces in ice-cold PBS. Intestinal epithelial cells were dissociated by incubation in HBSS (Sigma-Aldrich) containing 10 mm EDTA (Thermo Fisher Scientific), 1 mm DTT (Sigma-Aldrich) and 4% FBS with shaking at 130 rpm for 20 min at 37°C. The resulting cell suspension was passed through a 70 μm cell filter. The remaining tissues were enzymatically digested in RPMI 1640 containing 10 mm HEPES (Gibco), 0.5 mg/mL collagenase D (Sigma-Aldrich), 0.5 mg/mL DNase I (Sigma-Aldrich) and 4% FBS on a shaker at 90 rpm for 40 min at 37°C. After incubation, the cell mixture was filtered through a 70 μm strainer. Leukocytes were enriched by 40% Percoll gradient centrifugation and resuspended in PBS containing 2% FBS, followed by antibody incubation.

Flow Cytometry

A Zombie AquaTM Fixable Viability Kit (BioLegend, 423102) was used to exclude dead cells. Antibody staining was performed at 4°C with the following fluorochrome-conjugated mAbs according to standard methods: anti-mouse CD45 (APC/Cyanine7-conjugated, clone S18009F), anti-mouse CD3 (APC-conjugated, clone 17A2), anti-mouse NK1.1 (PE/Dazzle 594-conjugated, clone S17016D), anti-mouse TCRγδ (PE-conjugated, clone GL3), anti-mouse CD8a (PerCP-conjugated, clone 53–6.7), anti-mouse CD4 (Pacific Blue-conjugated, clone GK1.5), anti-human CD3 (BV711-conjugated, clone OKT3), anti-human CD56 (APC-conjugated, clone 5.1H11), anti-human CD4 (BUV737-conjugated, clone RPA-T4), anti-human CD8a (BUV396-conjugated, clone RPA-T8) and anti-human TCRβ (BV605-conjugated, clone IP26) antibodies.

For intracellular staining, the cells were incubated in complete medium supplemented with Cell Activation Cocktail (BioLegend, 423304) at 37°C for 4 h. The cells were permeabilized with the Cyto-Fast™ Fix/Perm Buffer Set (BioLegend, 426803) following the manufacturer's protocol. The fixed cells were incubated with anti-mouse/human granzyme B (FITC-conjugated, clone QA16A02; BV421-conjugated, clone GB11) and anti-human perforin (APC/Cyanine7-conjugated, clone dG9) antibodies. The data were acquired using a FACS Symphony A5 system (BD Biosciences) and analyzed using FlowJo X.

UEA-I Labeling

For Ulex europaeus agglutinin-I (UEA-I; Thermo Fisher Scientific) staining, the sections were incubated with rhodamine UEA-I for 1 h at 37 °C. The tissue sections were washed three times in PBS buffer and then stained with DAPI (BioLegend) for 5 min at room temperature. Images were acquired via a confocal microscope (Zeiss).

AB/PAS Staining

For glycan detection, periodic acid-Schiff (PAS) (Sigma-Aldrich) and alcian blue (AB) (Sigma-Aldrich) were used to stain general intestinal carbohydrate moieties.

DNA Extraction of Fecal Bacteria

Fecal samples were promptly frozen upon collection and stored at −80°C until analysis. The frozen fecal samples were subsequently and meticulously pulverized in liquid nitrogen using a mortar and pestle. The DNA from the bacterial sources was then extracted following the established protocol of the TGuide S96 Magnetic Soil/Stool DNA Kit (Tiangen Biotech).

16S rRNA Gene Sequencing and Microbiota Data Analysis

The 338F: 5'-ACTCCTACGGGAGGCAGCA-3' and 806R: 5'- GGACTACHVGGGTWTCTAAT-3' universal primer set was used to amplify the V3-V4 region of the 16S rRNA gene from the genomic DNA extracted from each sample. Both the forward and reverse 16S primers were tailed with sample-specific Illumina index sequences to allow for deep sequencing. The total PCR amplicons were purified with Agencourt AMPure XP Beads (Beckman Coulter) and quantified via a Qubit dsDNA HS Assay Kit and a Qubit 4.0 Fluorometer (Thermo Fisher Scientific). After the individual quantification step, amplicons were pooled in equal amounts. The raw data were analyzed by the QIIME2 platform. Sequences with similarity $\geq$ 97% were clustered into the same operational taxonomic units (OTUs) by USEARCH. Taxonomy annotation of the OTUs was performed based on the Naive Bayes classifier in QIIME2 using the SILVA database with a confidence threshold of 70%. Furthermore, we employed linear discriminant analysis (LDA) effect size (LEfSe) to test for significant taxonomic differences among the groups. A logarithmic LDA score of 4.0 was set as the threshold for discriminative features.

Fecal Metabolomics Profiling

An ultra-performance liquid chromatography coupled with tandem mass spectrometry (UPLC-MS/MS) system (ACQUITY UPLC-Xevo TQ-S, Waters Corp., Milford, MA, USA) was used to quantitate targeted metabolomics profiling of the fecal samples. Briefly, lyophilized fecal samples were homogenized with methanol containing an internal standard, and the resulting supernatant was obtained. Then, ice-cold 50% methanol solution was added to dilute the sample, and the supernatant mixed with internal standards for each sample was sealed before UPLC-MS/MS profiling. The instrument parameters were as follows: ACQUITY UPLC BEH C18 1.7 μM VanGuard pre-column (2.1×5 mm) and ACQUITY UPLC BEH C18 1.7 μM analytical column (2.1×100 mm); column temperature 40 °C; mobile phases A (water with 0.1% formic acid) and mobile phases B (acetonitrile: IPA, 70:30); and gradient conditions (0–1 min (5% B), 1–11 min (5–78% B), 11–13.5 min (78–95% B), 13.5–14 min (95–100% B), 14–16 min (100% B), 16–16.1 min (100–5% B), and 16.1–18 min (5% B)). The whole profiling process was performed at Metabo-Profile Corp. (Shanghai, China). The raw data files generated by UPLC-MS/MS were processed via MassLynx software (Waters) to perform peak integration, calibration, and quantitation for each metabolite. Quantitative data for each metabolite were presented in the Supplementary Table 5. The iMAP platform (Metabo-Profile) was used for statistical analyses. O2PLS analysis was performed via OmicShare tools, a free online platform for data analysis (https://www.omicshare.com/tools).

Barrier Function Assay

A 70 kDa fluorescein isothiocyanate (FITC)-dextran (Sigma-Aldrich, FD70-100MG) solution (200 μL of 5 mg/mL) was administered by oral gavage to the fasted mice. The mice were anesthetized 4 hours following gavage, after which blood was collected and centrifuged at 10,000 ×g for 5 minutes. Serum was collected to quantify fluorescence at an excitation wavelength of 485 nm and an emission wavelength of 535 nm by using Varioskan LUX (Thermo Fisher Scientific, Waltham, MA, USA).

Statistical Analysis

Statistical analysis was performed using GraphPad Prism 9.0 software (GraphPad Software, San Diego, CA, USA). Animal exclusion based on the identification of outliers (ROUT method) using GraphPad Prism 9.0 software was not performed for the data analyses. To determine the appropriate statistical tests, we initially assessed whether the data followed a Gaussian distribution. Parametric statistical tests were deemed appropriate and subsequently employed when the data exhibited both a normal distribution and similar variances between the groups being compared. In cases where the data did not conform to a normal distribution, nonparametric statistical tests were applied. Statistical significance was determined using two-tailed Student's t tests (unpaired) for comparisons between two groups. For multiple group comparisons, one-way ANOVA with Dunn's multiple comparison test was used. For multiple comparisons, two-way ANOVA with Sidak's multiple comparison test was used. All the data are presented as the mean ± standard error of the

mean (s.e.m). Significance levels are indicated as follows: *$0.01 < P < 0.05$, **$0.001 < P < 0.01$, ***$P < 0.001$. "ns" denotes no statistical significance.

Results

Elevated CD8$^+$ T Cell-Activation and Perforin Expression in IBD Patients and Mice

To explore the transcriptomic characteristics of patients with IBD, we analyzed the colonic bulk RNA sequencing and single-cell sequencing data of patients with IBD from public databases. Our analysis revealed an enrichment of genes associated with the cytotoxic pathway, suggesting that the activation of this pathway might contribute to the progression of IBD (Figure 1A and B). This finding indicated heightened activity of immune cells, such as cytotoxic T cells and natural killer (NK) cells, which employ molecules such as perforin and granzymes for cell killing. The levels of standard transcripts of *GZMB* and *PRF1* were significantly elevated in patients with UC (Figure 1C) and CD (Figure 1D). Single-cell sequencing analysis of CD8$^+$ T cells from the colon of UC patients identified nine distinct clusters (Figure 1E). Among these clusters, the proportion of the *PRF1*$^+$*GZMB*$^+$ cluster was significantly greater in UC patients than in healthy controls (Figure 1F). Furthermore, the expression levels of *PRF1* and *GZMB* in all CD8$^+$ T cells were significantly greater in UC patients than in healthy controls (Figure 1G). To validate the conclusions from the public database analysis, we examined peripheral blood mononuclear cells (PBMCs) from patients with IBD. We found that the proportions of perforin$^+$ CD8$^+$ T cells and GZMB$^+$ CD8$^+$ T cells were increased in the PBMCs of patients with IBD (Figure 1H, Supplementary Figure 1A–C). Similarly, the expression of perforin generated by CD8$^+$ T cells increased in the colon of DSS-induced colitis model mice (Figure 1I, Supplementary Figure 1D–F). In contrast, within the mesenteric lymph nodes and spleen, neither the proportion of CD8$^+$ T cells nor perforin production varied significantly (Supplementary Figure 1G–I). These observations collectively suggest the pivotal role of perforin generated by CD8$^+$ T cells in the context of intestinal inflammation.

Perforin Deficiency Alleviated Intestinal Inflammation in DSS-Induced Colitis

To determine whether the elevated level of perforin contribute to aggravated intestinal inflammation, we induced colitis in *Prf1*$^{-/-}$ mice by administering 2.5% DSS in the drinking water for 7 days. Compared with wild-type (WT) mice, *Prf1*$^{-/-}$ mice presented significantly reduced severity of IBD, characterized by decreased body weight loss (Figure 2A) and disease activity index (DAI) scores (Figure 2B). DSS-treated *Prf1*$^{-/-}$ mice presented increased colon length (Figure 2C and D) and reduced intestinal epithelial damage (Figure 2E). Moreover, we evaluated the integrity of the colonic mucosal layer and barrier in IBD mice. We characterized the function of goblet cells in *Prf1*$^{-/-}$ mice. PAS and Alcian blue staining revealed a reduced loss of goblet cells in *Prf1*$^{-/-}$ colitis mice (Figure 2F). An increase in mucus layer thickness was observed in the distal colon of *Prf1*$^{-/-}$ mice (Figure 2G). To assess intestinal barrier function in *Prf1*$^{-/-}$ mice, we focused on paracellular leakage and the integrity of the tight junction pathway via the use of 70 kDa dextran. Consistent with the goblet cell status, the reduced flux of dextran suggested an intact intestinal barrier in *Prf1*$^{-/-}$ mice (Figure 2H). The absence of perforin alleviated inflammatory responses, suggesting that perforin-mediated mucosal barrier damage plays a crucial role in the progression of DSS-induced colitis.

CD8$^+$ T Cell-Specific Perforin Deficiency Attenuated Colitis Pathology

To determine whether the absence of perforin in CD8$^+$ T cells can mitigate colitis, we established an adoptive transfer model using CD8$^+$ T lymphocytes. Naïve CD8$^+$ T cells (CD44^{low}CD62L$^+$CD8$^+$ T cells) from the spleens of WT or *Prf1*$^{-/-}$ mice were isolated and transferred intravenously into lymphopenic *Rag2*$^{-/-}\gamma c^{-/-}$ recipient mice (Figure 3A). The adoptive transfer of *Prf1*$^{-/-}$ CD8$^+$ T cells resulted in attenuated colitis, as evidenced by less weight loss in *Rag2*$^{-/-}\gamma c^{-/-}$ recipients during weeks 3–6 post-transfer (Figure 3B). The absence of perforin in CD8$^+$ T cells markedly reduced the severity of colitis, which was characterized by reduced colon weight and colonic wall thickness, and decreased inflammation in *Rag2*$^{-/-}\gamma c^{-/-}$ mice receiving *Prf1*$^{-/-}$ CD8$^+$ T cells (Figure 3C–E). These findings indicate that CD8$^+$ T-cell-derived perforin plays a critical role in exacerbating intestinal inflammation and support the notion of targeting perforin as a potential therapeutic strategy for treating IBD.

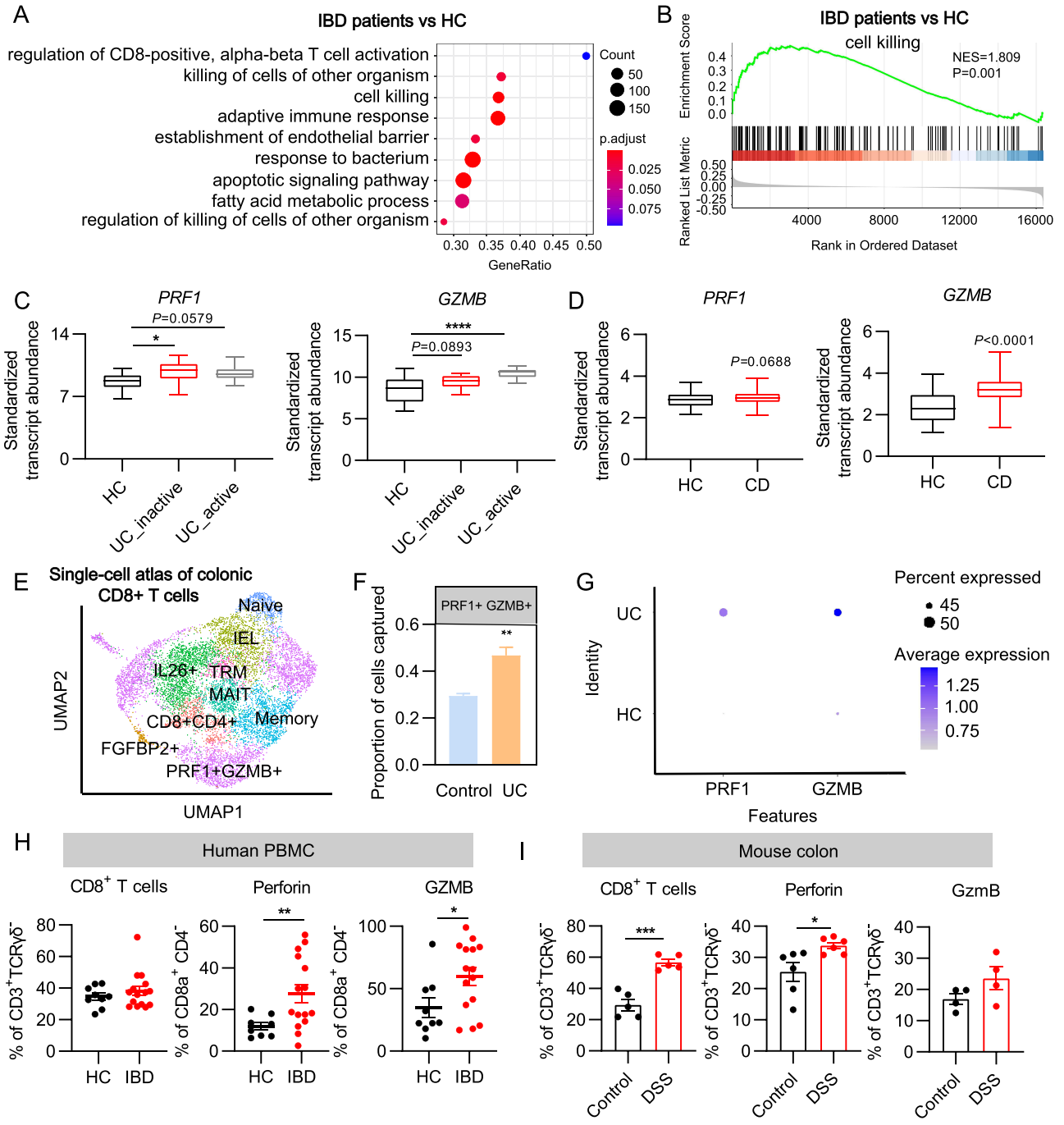

Figure 1 Elevated CD8$^+$ T cell-activation and perforin expression in IBD patients and mice. (**A**) GO.GSEA of GEO data (GEO accession: GSE53306) from healthy controls and patients with IBD. (**B**) Selected gene sets enriched in patients with IBD compared with healthy controls were plotted. (**C**) Standardized transcript abundance of *PRF1* and *GZMB* in healthy controls and UC patients during the active and inactive phases (GEO accession: GSE53306). (**D**) Standardized transcript abundance of *PRF1* and *GZMB* in healthy controls and CD patients (GEO accession: GSE93624). (**E**) UMAP plot visualization of colonic CD8$^+$ T-cell clusters detected in healthy controls and UC patients (GEO accession: GSE148837). (**F**) Changes in the composition of the PRF1$^+$GZMB$^+$CD8$^+$ subpopulation in healthy controls and UC patients. (**G**) Dot plot showing PRF1 and GZMB expression in UC patients and healthy controls. (**H**) Proportion of CD8$^+$ T cells and perforin$^+$ or GzmB$^+$ CD8$^+$ T cells among the PBMCs of healthy controls (n=9) and patients with IBD (n=15). (**I**) Proportion of CD8$^+$ T cells and perforin$^+$ or GzmB$^+$ CD8$^+$ T cells in the colons of control (n=4–6) and colitis mice (n=4–6). *0.01 < P < 0.05, **0.001 < P < 0.01, ***0.0001< P < 0.001, ****P < 0.0001.

Abbreviations: HC, healthy controls; IBD, inflammatory bowel disease; UC, ulcerative colitis; CD, Crohn's disease; GO, Gene Ontology; GSEA, Gene Set Enrichment Analysis.

https://doi.org/10.2147/JIR.S509875

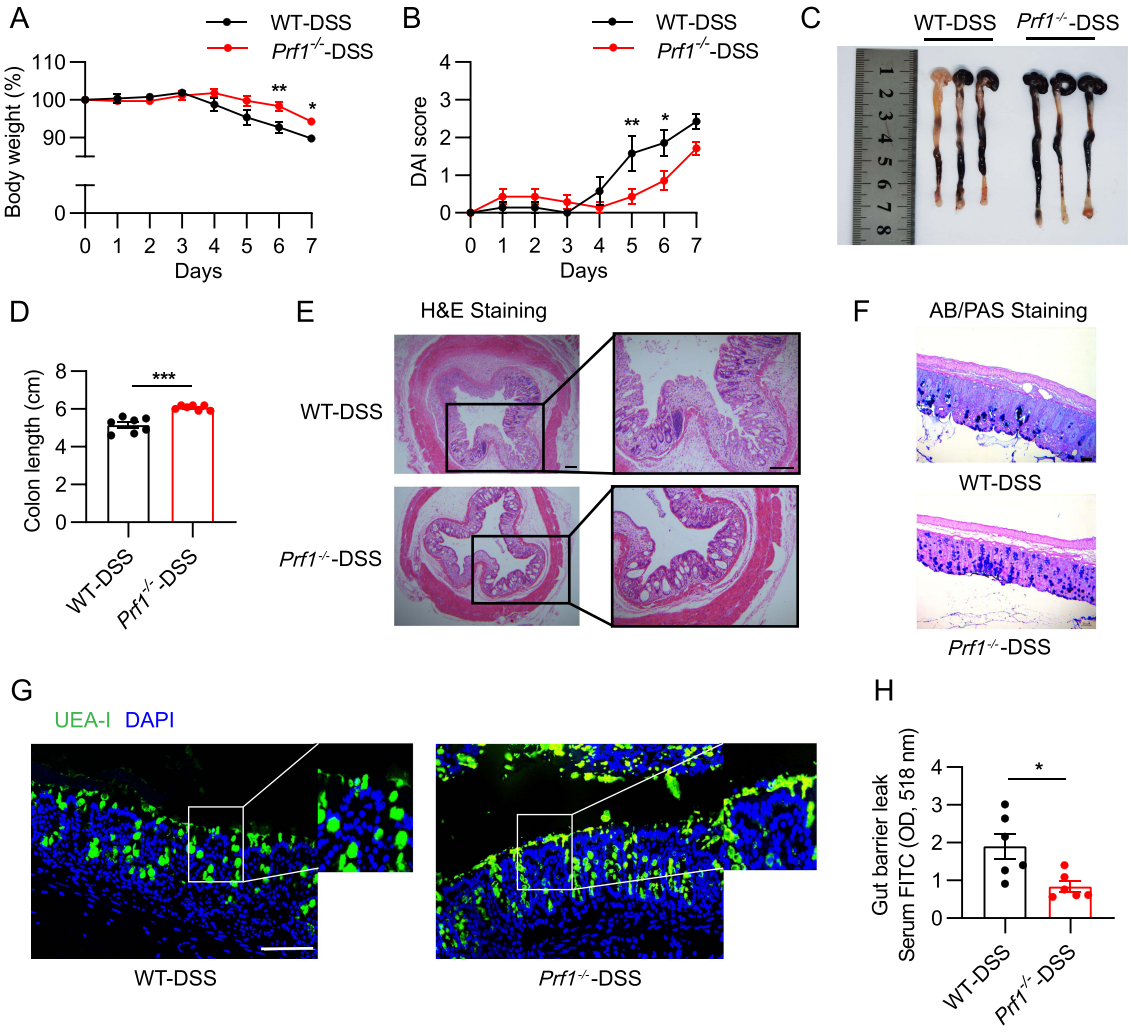

Figure 2 Perforin deficiency alleviated intestinal inflammation in DSS-induced colitis. (**A**) Body weights and (**B**) disease scores of WT (n=7) and *Prf1*$^{-/-}$ (n=7) mice given 2.5% DSS in the drinking water for 7 days. (**C**) Representative images of colon length in WT and *Prf1*$^{-/-}$ mice. (**D**) Colon lengths of WT (n=7) and *Prf1*$^{-/-}$ (n=7) mice with colitis. (**E**) Distal sections of the colon were examined by H&E staining. Scale bar = 100 μm. (**F**) Alcian blue/PAS staining of colons from WT and *Prf1*$^{-/-}$ mice with colitis. Scale bar = 50 μm. (**G**) Staining for UEA-I (immunofluorescence, green) in Carnoy's-fixed colonic sections from WT and *Prf1*$^{-/-}$ mice with colitis. Scale bar = 100 μm. (**H**) Detection of the absorbance in the serum of WT (n=6) and *Prf1*$^{-/-}$ (n=6) mice with colitis. *0.01 < *P* < 0.05, **0.001 < *P* < 0.01, ***0.0001< *P* < 0.001.
Abbreviations: H&E staining, hematoxylin-eosin staining; AB, alcian blue; PAS, periodic acid; UEA-I, ulex europaeus agglutinin.

Upregulated Expression of Hmgcs2 Increased β-Hydroxybutyrate Levels in Prf1$^{-/-}$ Mice

To elucidate the underlying mechanisms by which *Prf1* deficiency affects colitis in mice, we performed RNA sequencing on the colons of WT and *Prf1*$^{-/-}$ mice with DSS-induced colitis. We identified 99 upregulated and 121 downregulated DEGs in *Prf1*$^{-/-}$ mice (Supplementary Figure 2A). GSEA revealed that pathways associated with fatty acid metabolism were significantly enriched in *Prf1*$^{-/-}$ mice (Figure 4A). Given the downregulated enrichment of fatty acid metabolic pathways in patients with IBD (Supplementary Figure 2B), we hypothesized that the alleviation of enteritis in *Prf1*$^{-/-}$ mice might be related to metabolic changes. We then conducted a fecal metabolomic analysis. Small Molecule Pathway Database (SMPDB) analysis revealed enrichment of genes related to ketone body metabolism and fatty acid oxidation (Figure 4B). The loading plot and loading diagram provided insights into the correlation between specific metabolites and genes (Figure 4C, Supplementary Figure 2C). The metabolomic and transcriptomic loadings highlighted a significant association between numerous metabolites and genes, among which the gene encoding a key enzyme in fatty acid metabolism, *Hmgcs2*, and its metabolite β-hydroxybutyrate (BHB, also named 3-hydroxybutyric acid) were both enriched (Figure 4C). Considering recent studies reporting that BHB contributes to alleviating intestinal

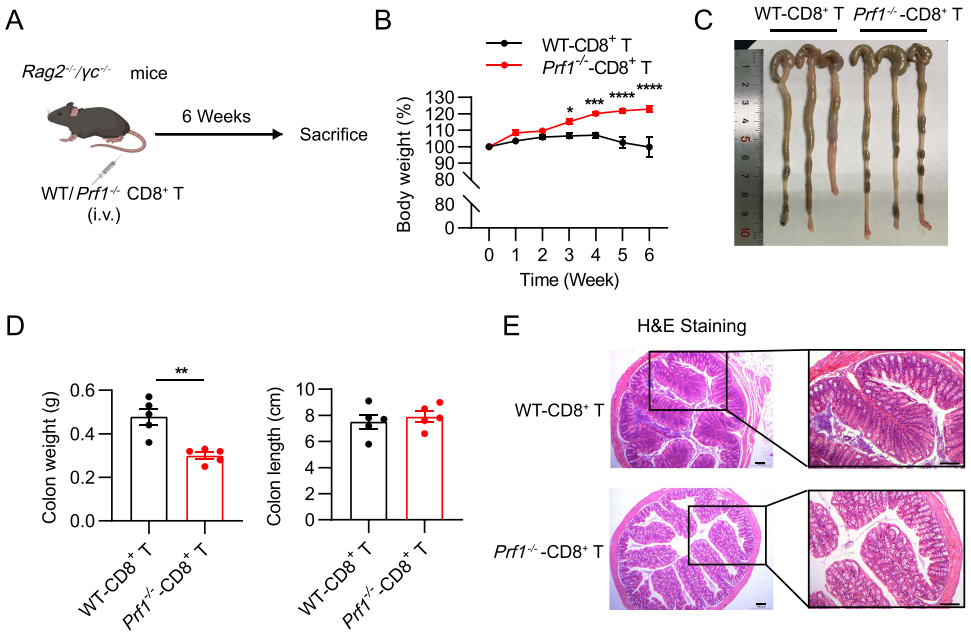

Figure 3 $CD8^+$ T cell-specific perforin deficiency attenuated colitis pathology. (**A**) Schematic illustration and timeline of the adoptive transfer-induced colitis model (created with BioRender.com). (**B**) Body weights of recipient $Rag2^{-/-}\gamma c^{-/-}$ mice receiving WT (n=5) or $Prf1^{-/-}$ (n=5) naïve $CD8^+$ T cells. (**C**) Representative images and (**D**) colon lengths and weights of recipient $Rag2^{-/-}\gamma c^{-/-}$ mice. (**E**) Representative H&E-stained sections of the colon of recipient $Rag2^{-/-}\gamma c^{-/-}$ mice. Scale bar = 100 μm. *0.01 < *P* < 0.05, **0.001 < *P* < 0.01, ***0.0001< *P* < 0.001, ****P < 0.0001.

inflammation,[17,18] we focused our attention on *Hmgcs2* and BHB. Several genes involved in fatty acid metabolism, such as *Hmgcs2, Pdk4, Acot2, Cyp4a10*, and *Acot1*, were upregulated in $Prf1^{-/-}$ mice with DSS-induced colitis (Figure 4D). A real-time PCR assay verified the significant increase in *Hmgcs2* and *Pdk4* mRNA levels in $Prf1^{-/-}$ mice (Figure 4E).

Hmgcs2 encodes the rate-limiting enzyme 3-hydroxy-3-methylglutaryl-CoA synthase 2 (HMGCS2) in the fatty acid metabolism pathway. HMGCS2 catalyzes the conversion of two acetyl-CoA molecules into 3-hydroxy-3-methylglutaryl-CoA (HMG-CoA), which is then cleaved by HMG-CoA lyase (HMGCL) to produce acetoacetate and another acetyl-CoA, which enters the ketone body synthesis cycle (Figure 4F). As depicted in Figure 4G, by analyzing the variations in metabolic products, we observed a significant increase in BHB production in $Prf1^{-/-}$ colitis mice compared with WT colitis mice. We also subsequently observed a marked increase in plasma BHB levels in $Prf1^{-/-}$ colitis model mice, which was consistent with the findings from the fecal metabolomic study (Figure 4H). To further investigate the role of BHB in colitis, we administered intraperitoneal injections of either vehicle or BHB to WT-DSS mice. The BHB-treated group exhibited increased colon length and reduced severity of colonic inflammation (Supplementary Figure 3A–D). Furthermore, we observed an upward trend in the *Firmicutes/Bacteroidetes* (F/B) ratio within the intestinal microbiota of the BHB-treated group (Supplementary Figure 3E), potentially associated with reduced inflammation.[19] The absence of *Prf1* resulted in an increase in *Hmgcs2* metabolic gene expression and BHB metabolism, likely contributing to the maintenance or repair of intestinal barrier function.

Prf1 Deficiency Affected the Composition of the Gut Microbiota in Mice with Colitis

In the intestine, fecal metabolic alterations consistently affect the composition and function of the gut microbiota through metabolism-microbiota interactions. Using 16S rRNA sequencing, we analyzed the gut microbiota composition of WT and $Prf1^{-/-}$ mice with DSS-induced colitis. A slight reduction in the number of OTUs, with no significant difference in the Chao1 index, Shannon index, or Simpson index, was observed in $Prf1^{-/-}$ mice with DSS-induced colitis (Figure 5A), suggesting a minor change in the intestinal flora diversity of $Prf1^{-/-}$ mice. Principal component analysis (PCA) of the gut microbiota composition revealed distinct clustering of WT and $Prf1^{-/-}$ DSS-induced colitis mice (Figure 5B). At the phylum level, significant alterations in the gut microbiota of WT and $Prf1^{-/-}$ DSS-induced colitis mice were observed (Figure 5C). Specifically, the *Firmicutes*/*Bacteroidetes* ratio significantly increased in $Prf1^{-/-}$ colitis model mice

https://doi.org/10.2147/JIR.S509875

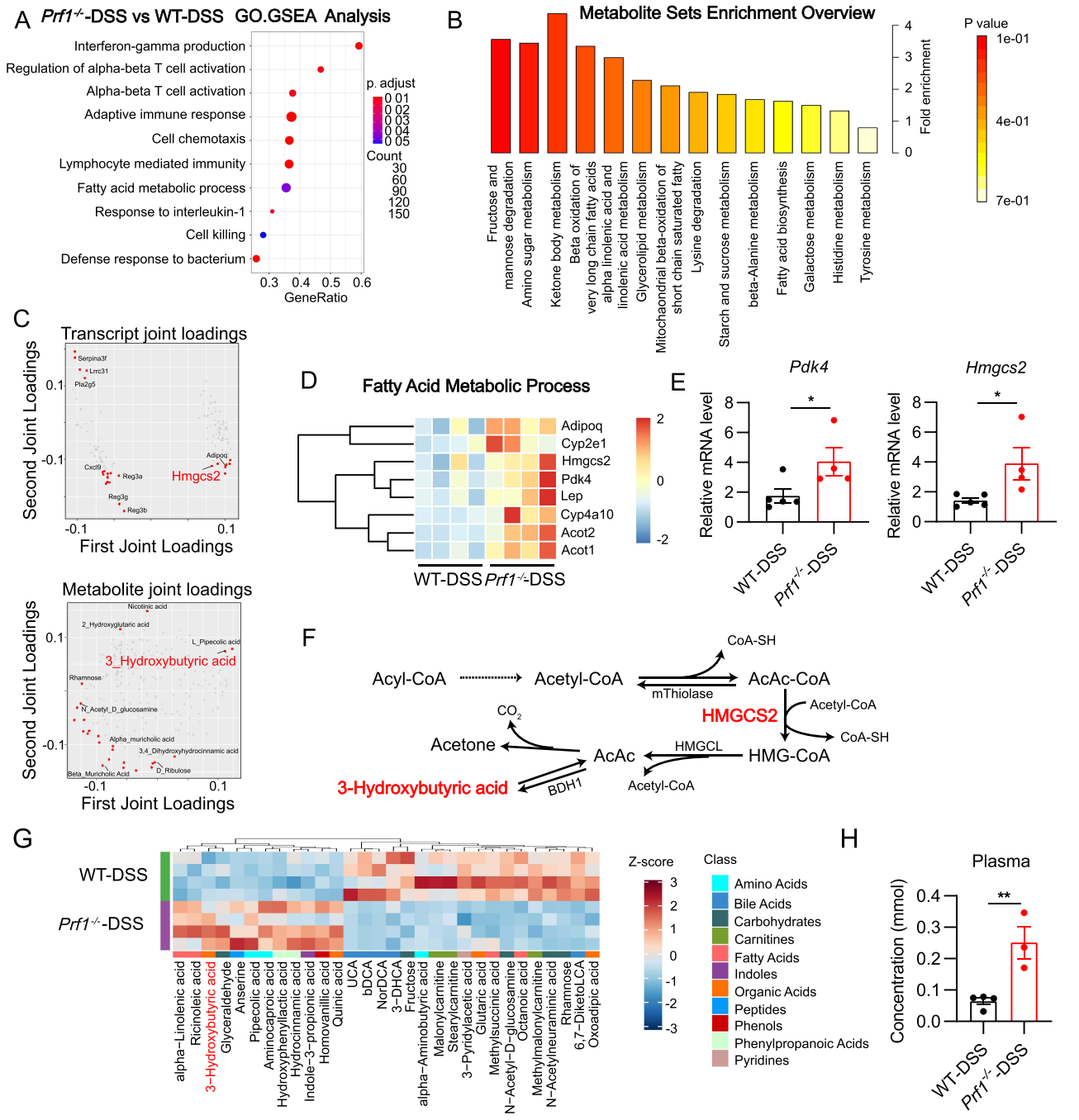

Figure 4 Upregulated expression of *Hmgcs2* increased β-hydroxybutyrate levels in *Prf1*$^{-/-}$ mice. (**A**) GO.GSEA of bulk RNA-seq data from colons of WT (n=4) and *Prf1*$^{-/-}$ mice (n=4) after DSS treatment. (**B**) SMPDB (Small Molecule Pathway Database) analysis of the metabolome in the feces of WT (n=4) and *Prf1*$^{-/-}$ mice (n=4) after DSS treatment. (**C**) O2PLS load diagram. The transcriptome data are at the top, and the metabolome data are at the bottom. Each dot represents a metabolite or a gene. The horizontal coordinate is the first dimensional coordinate of the joint part, and the vertical coordinate is the second-dimensional coordinate of the joint part. The greater the absolute value of an element in the coordinates, the greater the correlation between this element and another omics. (**D**) Heatmap of fatty acid metabolic process-related gene expression according to RNA sequencing. (**E**) Quantitative real-time PCR (qPCR) detection of *Pdk4* and *Hmgcs2* mRNA expression levels in the colons of WT (n=5) and *Prf1*$^{-/-}$ (n=4) mice subjected to DSS. (**F**) The synthetic metabolic pathway of β-hydroxybutyrate. (**G**) Heatmap of the metabolite content in feces. (**H**) β-hydroxybutyrate concentration in the plasma of WT (n=4) and *Prf1*$^{-/-}$ (n=3) colitis model mice. *0.01 < *P* < 0.05, **0.001 < *P* < 0.01.

(Figure 5D). At the genus level, members of the anaerobic bacteria *Alloprevotella* and *Parabacteroides*, which are involved in host metabolism, including energy intake, short-chain fatty acid (SCFA) production, and maintenance of intestinal barrier function,[20,21] presented increased relative abundance in *Prf1*$^{-/-}$ colitis mice (Figure 5E and F). These

 https://doi.org/10.2147/JIR.S509875

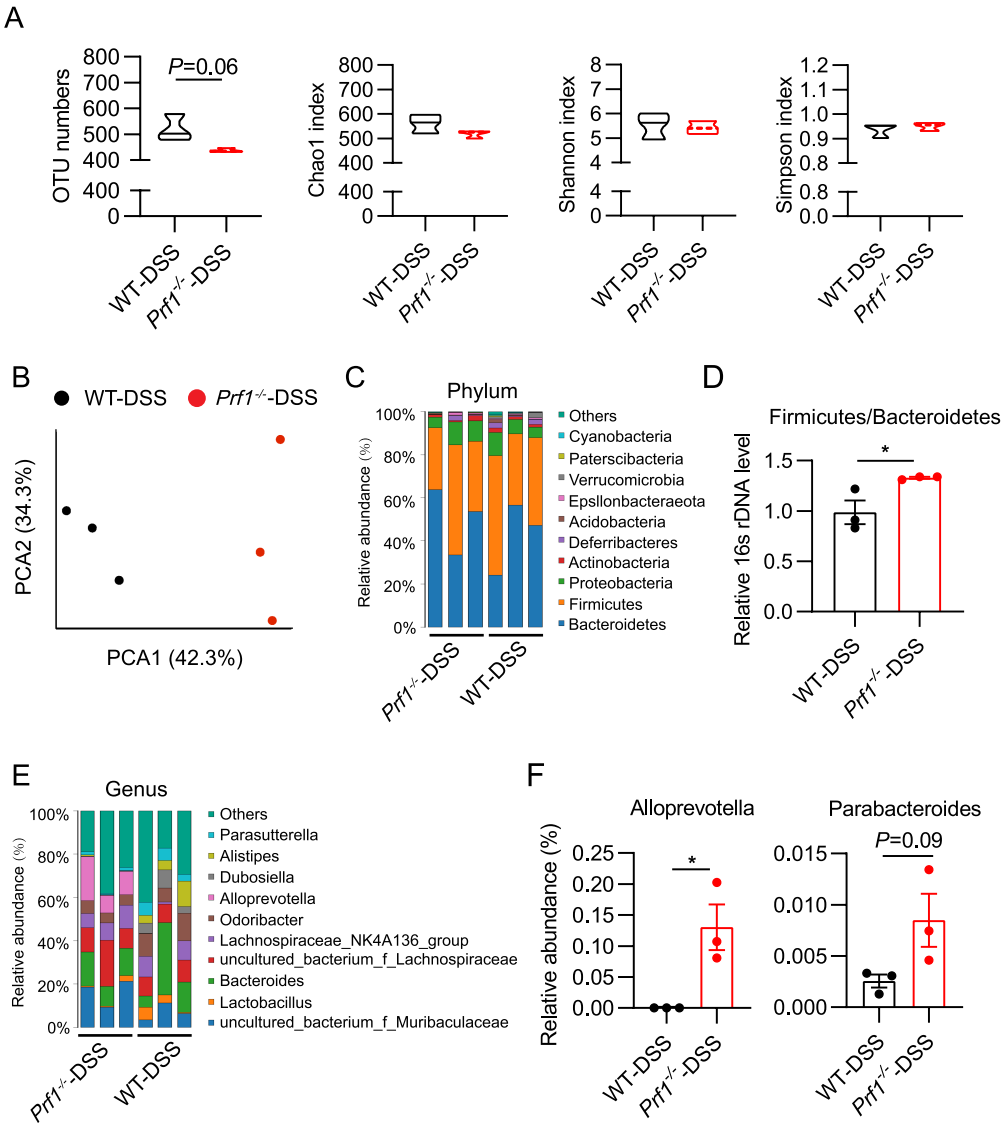

Figure 5 *Prf1* deficiency affected the composition of the gut microbiota in mice with colitis. (**A**) OTU numbers, Chao1 index, Shannon index and Simpson index of the microbiota in the feces of WT (n=3) and *Prf1*$^{-/-}$ (n=3) mice with colitis. (**B**) Principal component analysis of the intestinal microbiota in WT and *Prf1*$^{-/-}$ mice with colitis. (**C**) Analysis of specific bacterial 16S rRNA to detect commensal diversity in WT and *Prf1*$^{-/-}$ mice at the phylum level. (**D**) Real-time PCR confirmation of the microbiota composition in WT (n=3) and *Prf1*$^{-/-}$ (n=3) mice with colitis. (**E**) Analysis of specific bacterial 16S rRNA to detect commensal diversity in WT and *Prf1*$^{-/-}$ mice at the genus level. (**F**) Genus selected from mice with given treatment. *0.01 < *P* < 0.05.
Abbreviation: OTUs, operational taxonomic units.

data indicate that *Prf1* deficiency affects the composition of the gut microbiota in mice with colitis, which is characterized by increased *Alloprevotella* and *Parabacteroides* abundances.

Inhibition of HMGCS2 Increased the Susceptibility of Prf1$^{-/-}$ Mice to DSS-Induced Colitis by Worsening the Gut Microbiota Ecology

To further demonstrate the role of HMGCS2 in intestinal inflammation and dysbiosis, we injected the HMGCS2 inhibitor hymeglusin intraperitoneally into *Prf1*$^{-/-}$ mice and examined DSS-induced acute colitis. After HMGCS2 inhibition, *Prf1*$^{-/-}$ mice lost more weight and showed higher DAI scores compared to controls upon DSS challenge (Figure 6A and B). Additionally, *Prf1*$^{-/-}$ mice treated with HMGCS2 inhibitor presented shorter colon lengths (Figure 6C and D) and more severe intestinal damage (Figure 6E). After HMGCS2 was inhibited, the BHB produced by host fatty acid metabolism was reduced, resulting in increased susceptibility of *Prf1*$^{-/-}$ mice to DSS-induced colitis. Since metabolic

https://doi.org/10.2147/JIR.S509875

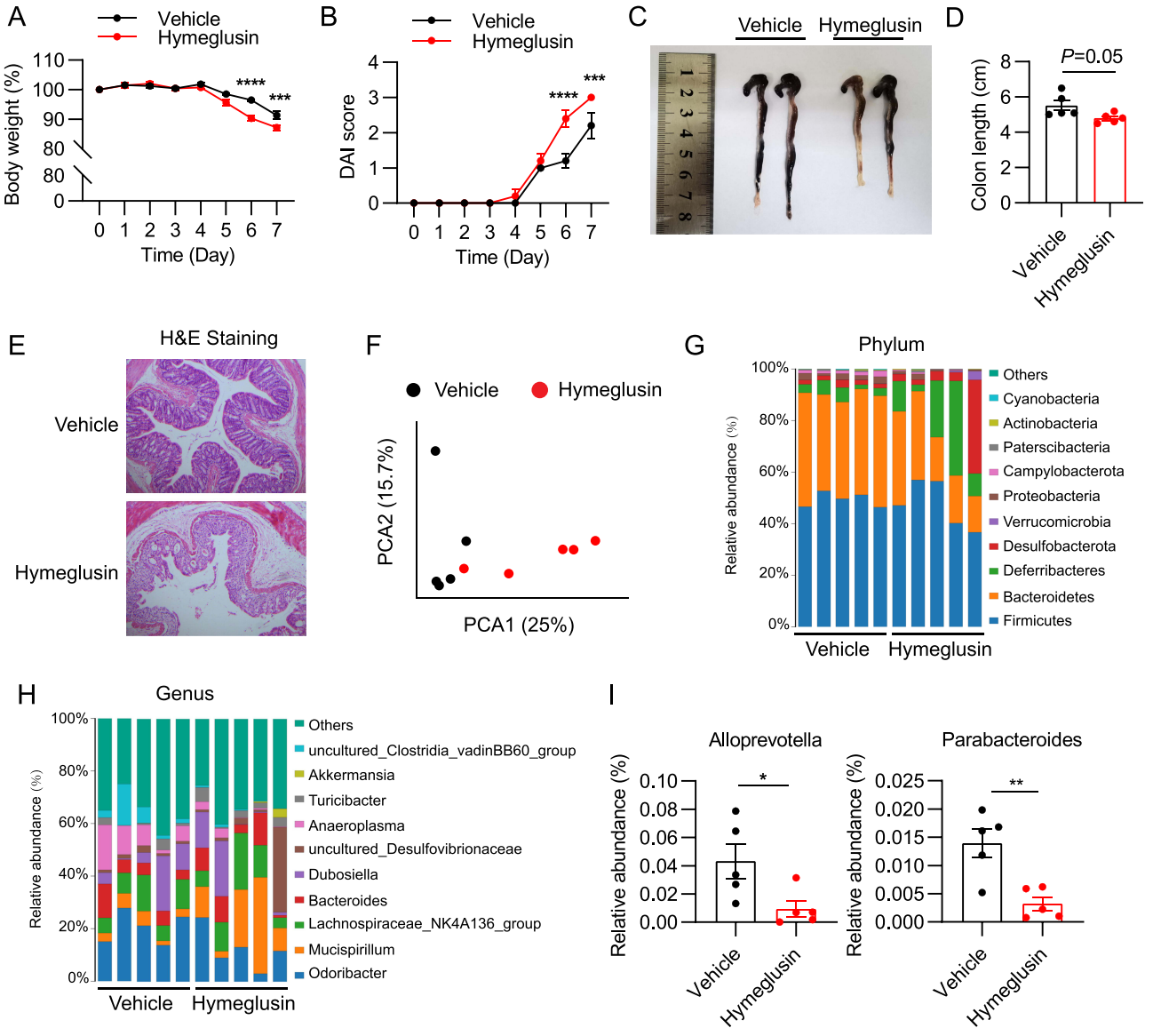

Figure 6 Inhibition of HMGCS2 increased the susceptibility of *Prf1*$^{-/-}$ mice to DSS-induced colitis by worsening the gut microbiota ecology. (**A**) Body weights and (**B**) disease scores of *Prf1*$^{-/-}$ mice injected with vehicle (n=5) or hymeglusin (n=5) followed by 2.5% DSS in the drinking water for 7 days. (**C**) Representative images and (**D**) colon lengths of *Prf1*$^{-/-}$ mice after vehicle or hymeglusin injection. (**E**) Distal sections of the colons examined by H&E staining. Scale bar = 100 μm. (**F**) Principal component analysis of the intestinal microbiota of *Prf1*$^{-/-}$ colitis mice receiving vehicle or hymeglusin. (**G** and **H**) Analysis of specific bacterial 16S rRNA to detect commensal diversity at (**G**) the phylum level and (**H**) the genus level. (**I**) Genus selected from mice with given treatment. *0.01 < *P* < 0.05, **0.001 < *P* < 0.01, ***0.0001< *P* < 0.001, ****P* < 0.0001.

changes cause variation in the intestinal flora composition, 16S rRNA analysis suggested significant alterations in the gut microbiota at the phylum and genus levels in *Prf1*$^{-/-}$ DSS-induced colitis mice after HMGCS2 inhibition compared with controls (Figure 6F–H). The diversity of the intestinal microbiota was reduced in *Prf1*$^{-/-}$ mice treated with hymeglusin (Supplementary Figure 4A–D). Notably, the abundance of *Alloprevotella* and *Parabacteroides*, which were previously increased in *Prf1*$^{-/-}$ DSS-induced colitis mice (Figure 5F), was significantly reduced upon the inhibition of HMGCS2 (Figure 6I). These data demonstrated that HMGCS2 inhibition increased the susceptibility of *Prf1*$^{-/-}$ mice to DSS-induced colitis by affecting the composition of the gut microbiota.

Discussion

In the present study, we revealed an enrichment of genes associated with CD8^{+} T cells and cell killing in the intestines of patients with IBD. Recent studies on cytotoxic CD8^{+} T cells in IBD also suggested their involvement in the course of the

disease.[7] $CD8^+$ T cells depend on the synergy between perforin and granzymes to cause target cell death.[8] We verified that the proportion of cytotoxic $CD8^+$ T cells highly expressing perforin and granzyme B was significantly increased in patients with IBD and mice with colitis. Moreover, this study revealed that perforin exacerbated dysbiosis and IBD by inhibiting BHB production in colonic epithelial cells.

The phenotypic and mechanistic characterization of various granzymes participating in IBD is not exactly the same. The upregulated expression of granzyme B can be used as a promising biomarker to detect active IBD, while granzyme M can act directly to induce colonic protection.[22,23] The pore-forming activity of perforin is a prerequisite for the delivery of granzymes into the cytosol of target cells. Thus, we evaluated whether perforin regulates colonic inflammation. In this study, the role of perforin was illustrated by the fact that *Prf1*$^{-/-}$ mice were significantly protected from DSS-induced colitis and developed a decreased histological score. Perforin deficiency in $CD8^+$ T cells significantly relieved colitis in an adoptive transfer model. Early studies have shown that perforin deficiency attenuates chronic inflammation-induced colitis-associated cancer,[24] whereas the mechanism by which perforin promotes intestinal inflammation has not been fully elucidated.

Metabolites secreted by the host or microbiota play critical roles in the progression of intestinal diseases. BHB is a small ketone body molecule, synthesized from fatty acids in both the liver and the gut epithelium. HMGCS2, the mitochondrial rate-limiting enzyme, is responsible for BHB production and specifically expressed in epithelial cells.[25] To maintain colonization, gut bacteria require nutrient inputs, including ingested food, host-synthesized intestinal mucus, and host circulating metabolites.[26–28] Recent work has shown that BHB, lactate, and urea stand out for passing from the host to the gut microbiome.[29] Thus, maintaining HMGCS2 expression is crucial for supplying BHB to the microbiota. We confirmed that perforin deficiency increased fatty acid metabolism and increased the expression of *Pdk4*, a sensitive marker of fatty acid oxidation[30] and *Hmgcs2*, a mitochondrial enzyme that catalyzes the first irreversible step in ketogenesis,[25] which could lead to the accumulation of BHB.

The intestinal mucosa is colonized by massive commensal, opportunistic pathogenic, and pathogenic microorganisms.[31] An imbalance in microbial homeostasis leads to the colonization and invasion of opportunistic pathogens, which promotes the development of IBD.[32] BHB can promote the ability of the commensal microflora to compete with the pathogenic microflora for ecological niches and nutrient resources, which is thought to inhibit the proliferation and invasion of the latter.[33] Since increased BHB levels were observed in this study, it is plausible that beneficial gut microbiota ecology was observed in *Prf1*$^{-/-}$ mice with colitis. These changes included the expansion of beneficial commensal species such as *Alloprevotella* and *Parabacteroides*. Recent studies have shown that *Alloprevotella*, which is generally considered as a short-chain fatty acid producer, can promote weight gain and reduce intestinal inflammation and diarrhea.[20,34] The enrichment of *Parabacteroides* in the gut protects both acute and chronic models of colitis induction.[21] Notably, the trend of changes in the gut microbiota composition observed in *Prf1*$^{-/-}$ mice with colitis was reversed by the HMG-CoA synthase inhibitor hymeglusin, which could lower BHB accumulation.[35] As a result, the administration of hymeglusin aggravated colitis in *Prf1*$^{-/-}$ mice. Therefore, we propose that the upregulation of BHB is responsible for the changes in microbiota composition observed in *Prf1*$^{-/-}$ mice with colitis.

We confirmed that perforin deficiency ameliorated mucosal barrier damage by increasing the expression of acidic mucins and the thickness of the mucus layer and reducing intestinal permeability in mice with colitis. The intestinal barrier is a dynamic entity that is lined by intestinal epithelial cells covered with a hyperviscous gel-forming mucus layer.[36] When epithelial cells are damaged or undergo apoptosis, a high-capacity and permissive pathway form.[37,38] $CD8^+$ T cells play an essential role as causative factors of increased intestinal permeability.[39] Research has shown that reduced chronic colitis in perforin-deficient mice is associated with a decrease in epithelial cell apoptosis.[24] Therefore, the alteration of intestinal permeability may be caused by the apoptosis of intestinal epithelial cells induced by perforin derived from $CD8^+$ T cells. Furthermore, BHB also plays a crucial role in the regulation of intestinal epithelial homeostasis. BHB facilitates mucosal repair through promoting intestinal epithelial proliferation and reducing crypt loss in DSS-exposed colons.[17] Additionally, BHB promotes goblet cell differentiation, as revealed by increased expression of MUC2.[40] Since mucins with terminal sialic acid and sulfate residues can be cleaved by bacterial sialidases and glycosulfatases, the loss of acidic mucins may lead to alterations in bacterial composition.[16,41] These results highlighted that perforin generated by $CD8^+$ T cells disrupted the integrity of the intestinal barrier and homeostasis through distinct

effects. These include disruption of the epithelial barrier by promoting the apoptosis of epithelial cells and destruction of the mucus barrier through downregulation of BHB expression.

This study effectively aimed to elucidate the role of perforin in the pathogenesis of IBD. The strengths of this design included the use of multiple methodologies, such as metabolic profiling and 16S rRNA sequencing, providing a comprehensive analysis of inflammation and microbiota. While our study provides mechanistic insights into perforin-mediated BHB suppression and its role in dysbiosis, these conclusions are derived solely from acute-colitis murine models. Despite the limited sample size in our IBD patient cohort, we observed significant upregulation of perforin and granzyme B (GZMB) expression in circulating CD8+ T lymphocytes. This finding provided preliminary experimental validation of our bioinformatics predictions, highlighting promising avenues for developing innovative immunological biomarkers in clinical applications. Notably, the lack of significant differences in circulating CD8+ T cell proportions between groups may reflect insufficient statistical power due to sample size constraints. These observations underscored the necessity for future large-scale investigations to validate and extend our findings.

These data further emphasized the important role of the interaction between host metabolites and the gut microbiota in the pathogenesis of IBD, with significant consequences for therapeutic strategies. We proposed the use of inhibitors to target the production of perforin or antisense oligonucleotides to suppress the expression of perforin, thereby mitigating IBD. The levels of perforin or BHB may be a biomarker for prognosis and personalized treatment. Despite challenges like gut-specific perforin inhibitors or BHB delivery, this link paves the way for metabolism-centric IBD therapies.

Conclusion

In this study, we found that the proportion of cytotoxic $CD8^+$ T cells expressing high levels of perforin was significantly increased in both IBD patients and colitis model mice. Perforin deficiency in $CD8^+$ T cells reduced the severity of colitis in mice. Additionally, the levels of metabolic products were altered in perforin-deficient colitis model mice, with a significant increase in the content of BHB, which improved colitis by inhibiting inflammation and correcting dysbiosis. These findings indicate that perforin aggravates colonic inflammation in individuals with IBD. The underlying mechanism is closely related to gut microbiota disequilibrium regulated by BHB metabolism in colonic epithelial cells.

Data Sharing Statement

The RNA sequencing data from this study can be found at the China National Center for Bioinformation (CNCB) under accession number PRJCA026385. 16S rRNA sequencing data are deposited on the SRA of CNCB under accession number PRJCA028282. The metabolomics data are shown in the supplementary materials. Further information and requests for resources and reagents should be directed to and will be fulfilled by the lead contact, Dan Tian (tiand@ccmu.edu.cn).

Ethics Approval and Consent to Participate

The Research Ethics Committee of Beijing Friendship Hospital, Capital Medical University approved the study design (Ethical permit No. 2022-P2-428-01). The study was carried out in accordance with the Declaration of Helsinki. All patients and controls signed informed consent for participation.

Acknowledgments

We are grateful to the Laboratory Animal Center, Beijing Friendship Hospital, for providing animal care. We thank the Institute of Clinical Medicine, Beijing Friendship Hospital, for providing instruments for the experiments.

Funding

This work was supported by the National Natural Science Foundation of China (No. 82270606, No. 82171823, No. 82300618), R&D Program of Beijing Municipal Education Commission (No. KZ202210025036), Beijing Municipal Administration of Hospitals' Ascent Plan (No. DFL20220103), the Youth Beijing Scholar (No. 035), the National Key Technologies R&D Program (No. 2015BAI13B09), Beijing Natural Science Foundation (No. 7232035), Beijing Nova Program (No. 20240484501), and Distinguished Young Scholars from Beijing Friendship Hospital (No. yyqcjh2022-4).

Disclosure

The authors declare that they have no known competing financial interests or personal relationships that could have appeared to influence the work reported in this paper.

References

1. Kaplan GG. The global burden of IBD: from 2015 to 2025. *Nat Rev Gastroenterol Hepatol*. 2015;12(12):720–727. doi:10.1038/nrgastro.2015.150
2. Neurath MF. Cytokines in inflammatory bowel disease. *Nat Rev Immunol*. 2014;14(5):329–342. doi:10.1038/nri3661
3. Liu S, Zhao W, Lan P, Mou X. The microbiome in inflammatory bowel diseases: from pathogenesis to therapy. *Protein and Cell*. 2020;12(5):331–345. doi:10.1007/s13238-020-00745-3
4. Neurath MF. Targeting immune cell circuits and trafficking in inflammatory bowel disease. *Nat Immunol*. 2019;20(8):970–979. doi:10.1038/s41590-019-0415-0
5. Gravina AG, Pellegrino R, Esposito A, et al. The JAK-STAT pathway as a therapeutic strategy in cancer patients with immune checkpoint inhibitor-induced colitis: a narrative review. *Cancers*. 2024;16(3):611. doi:10.3390/cancers16030611
6. Pellegrino R, Palladino G, Imperio G, Gravina AG. The growing potential of tofacitinib in immune checkpoint inhibitor-induced colitis: identifying remaining puzzle pieces. *Explor Immunol*. 2024;4:770–779. doi:10.37349/ei
7. Casalegno Garduno R, Dabritz J. New insights on CD8(+) T cells in inflammatory bowel disease and therapeutic approaches. *Front Immunol*. 2021;12:738762. doi:10.3389/fimmu.2021.738762
8. Voskoboinik I, Whisstock JC, Trapani JA. Perforin and granzymes: function, dysfunction and human pathology. *Nat Rev Immunol*. 2015;15(6):388–400. doi:10.1038/nri3839
9. Nancey S, Holvöet S, Graber I, et al. CD8+ cytotoxic T cells induce relapsing colitis in normal mice. *Gastroenterology*. 2006;131(2):485–496. doi:10.1053/j.gastro.2006.05.018
10. Cheng S, Hu J, Wu X, et al. Altered gut microbiome in FUT2 loss-of-function mutants in support of personalized medicine for inflammatory bowel diseases. *J Genet Genome*. 2021;48(9):771–780. doi:10.1016/j.jgg.2021.08.003
11. Weingarden AR, Vaughn BP. Intestinal microbiota, fecal microbiota transplantation, and inflammatory bowel disease. *Gut Microbes*. 2017;8(3):238–252. doi:10.1080/19490976.2017.1290757
12. Schirmer M, Garner A, Vlamakis H, Xavier RJ. Microbial genes and pathways in inflammatory bowel disease. *Nat Rev Microbiol*. 2019;17(8):497–511. doi:10.1038/s41579-019-0213-6
13. Liang L, Liu L, Zhou W, et al. Gut microbiota-derived butyrate regulates gut mucus barrier repair by activating the macrophage/WNT/ERK signaling pathway. *Clin Sci*. 2022;136(4):291–307. doi:10.1042/cs20210778
14. Li G, Lin J, Zhang C, et al. Microbiota metabolite butyrate constrains neutrophil functions and ameliorates mucosal inflammation in inflammatory bowel disease. *Gut Microbes*. 2021;13(1). doi:10.1080/19490976.2021.1968257
15. Pan Y, Tian D, Wang H, et al. Inhibition of perforin-mediated neurotoxicity attenuates neurological deficits after ischemic stroke. *Front Cell Neurosci*. 2021;15. doi:10.3389/fncel.2021.664312
16. Liang W, Peng X, Li Q, et al. FAM3D is essential for colon homeostasis and host defense against inflammation associated carcinogenesis. *Nat Commun*. 2020;11(1). doi:10.1038/s41467-020-19691-z
17. Huang C, Wang J, Liu H, et al. Ketone body β-hydroxybutyrate ameliorates colitis by promoting M2 macrophage polarization through the STAT6-dependent signaling pathway. *BMC Med*. 2022;20(1). doi:10.1186/s12916-022-02352-x
18. Yan X, Liu XY, Zhang D, et al. Construction of a sustainable 3-hydroxybutyrate-producing probiotic Escherichia coli for treatment of colitis. *Cell mol Immunol*. 2021;18(10):2344–2357. doi:10.1038/s41423-021-00760-2
19. Stojanov S, Berlec A, Štrukelj B. The influence of probiotics on the firmicutes/bacteroidetes ratio in the treatment of obesity and inflammatory bowel disease. *Microorganisms*. 2020;8(11):1715. doi:10.3390/microorganisms8111715
20. Deng L, Wojciech L, Png CW, et al. Colonization with ubiquitous protist Blastocystis ST1 ameliorates DSS-induced colitis and promotes beneficial microbiota and immune outcomes. *NPJ Biofilms Microbiomes*. 2023;9(1). doi:10.1038/s41522-023-00389-1
21. Gaifem J, Mendes-Frias A, Wolter M, et al. Akkermansia muciniphila and Parabacteroides distasonis synergistically protect from colitis by promoting ILC3 in the gut. *mbio*. 2024;15(4):e0007824. doi:10.1128/mbio.00078-24
22. Heidari P, Haj-Mirzaian A, Prabhu S, Ataeinia B, Esfahani SA, Mahmood U. Granzyme B PET imaging for assessment of disease activity in inflammatory bowel disease. *J Nucl Med*. 2024;65(7):1137–1143. doi:10.2967/jnumed.123.267344
23. Souza-Fonseca-Guimaraes F, Krasnova Y, Putoczki T, et al. Granzyme M has a critical role in providing innate immune protection in ulcerative colitis. *Cell Death Dis*. 2016;7(7):e2302. doi:10.1038/cddis.2016.215
24. Waldner MJ, Wirtz S, Becker C, et al. Perforin deficiency attenuates inflammation and tumor growth in colitis-associated cancer. *Inflamm Bowel Dis*. 2010;16(4):559–567. doi:10.1002/ibd.21107
25. Cheng C-W, Biton M, Haber AL, et al. Ketone body signaling mediates intestinal stem cell homeostasis and adaptation to diet. *Cell*. 2019;178(5):1115–1131.e15. doi:10.1016/j.cell.2019.07.048
26. Desai MS, Seekatz AM, Koropatkin NM, et al. A dietary fiber-deprived gut microbiota degrades the colonic mucus barrier and enhances pathogen susceptibility. *Cell*. 2016;167(5):1339–1353.e21. doi:10.1016/j.cell.2016.10.043
27. Sicard J-F, Le Bihan G, Vogeleer P, Jacques M, Harel J. Interactions of intestinal bacteria with components of the intestinal mucus. *Front Cell Infect Microbiol*. 2017;7. doi:10.3389/fcimb.2017.00387
28. Scheiman J, Luber JM, Chavkin TA, et al. Meta-omics analysis of elite athletes identifies a performance-enhancing microbe that functions via lactate metabolism. *Nature Med*. 2019;25(7):1104–1109. doi:10.1038/s41591-019-0485-4
29. Zeng X, Xing X, Gupta M, et al. Gut bacterial nutrient preferences quantified in vivo. *Cell*. 2022;185(18):3441–3456.e19. doi:10.1016/j.cell.2022.07.020
30. Pettersen IKN, Tusubira D, Ashrafi H, et al. Upregulated PDK4 expression is a sensitive marker of increased fatty acid oxidation. *Mitochondrion*. 2019;49:97–110. doi:10.1016/j.mito.2019.07.009

31. Kayama H, Okumura R, Takeda K. Interaction between the microbiota, epithelia, and immune cells in the intestine. *Ann Rev Immunol*. 2020;38 (1):23–48. doi:10.1146/annurev-immunol-070119-115104
32. Qiu P, Ishimoto T, Fu L, Zhang J, Zhang Z, Liu Y. The gut microbiota in inflammatory bowel disease. *Front Cell Infect Microbiol*. 2022;12. doi:10.3389/fcimb.2022.733992
33. Qi J, Gan L, Fang J, et al. Beta-hydroxybutyrate: a dual function molecular and immunological barrier function regulator. *Front Immunol*. 2022;13. doi:10.3389/fimmu.2022.805881
34. Chen H, Jia Z, He M, et al. Arula-7 powder improves diarrhea and intestinal epithelial tight junction function associated with its regulation of intestinal flora in calves infected with pathogenic Escherichia coli O1. *Microbiome*. 2023;11(1). doi:10.1186/s40168-023-01616-9
35. Lindsay RT, Dieckmann S, Krzyzanska D, et al. β-hydroxybutyrate accumulates in the rat heart during low-flow ischaemia with implications for functional recovery. *eLife*. 2021;10. doi:10.7554/eLife.71270
36. Paone P, Cani PD. Mucus barrier, mucins and gut microbiota: the expected slimy partners? *Gut*. 2020;69(12):2232–2243. doi:10.1136/gutjnl-2020-322260
37. Odenwald MA, Turner JR. The intestinal epithelial barrier: a therapeutic target? *Nat Rev Gastroenterol Hepatol*. 2016;14(1):9–21. doi:10.1038/nrgastro.2016.169
38. Liang B, Zhong Y, Huang Y, et al. Underestimated health risks: polystyrene micro- and nanoplastics jointly induce intestinal barrier dysfunction by ROS-mediated epithelial cell apoptosis. *Part Fibre Toxicol*. 2021;18(1). doi:10.1186/s12989-021-00414-1
39. Labarta-Bajo L, Nilsen SP, Humphrey G, et al. Type I IFNs and CD8 T cells increase intestinal barrier permeability after chronic viral infection. *J Exp Med*. 2020;217(12). doi:10.1084/jem.20192276
40. Wang Q, Zhou Y, Rychahou P, et al. Ketogenesis contributes to intestinal cell differentiation. *Cell Death Differ*. 2016;24(3):458–468. doi:10.1038/cdd.2016.142
41. Corfield AP, Wagner SA, Clamp JR, Kriaris MS, Hoskins LC. Mucin degradation in the human colon: production of sialidase, sialate O-acetylesterase, N-acetylneuraminate lyase, arylesterase, and glycosulfatase activities by strains of fecal bacteria. *Infect Immun*. 1992;60 (10):3971–3978. doi:10.1128/iai.60.10.3971-3978.1992